Analysis of reconstructions obtained solving l^p-penalized minimization problems

Flavia Lenti, *Student Member, IEEE,* Ferdinando Nunziata, *Senior Member, IEEE,* Claudio Estatico and Maurizio Migliaccio, *Senior Member, IEEE*

Abstract

Most of the inverse problems arising in applied electromagnetics come from an underdetermined direct problem, this is the case, for instance, of spatial resolution enhancement. This implies that no unique inverse operator exists; therefore, additional constraints must be imposed on the sought solution. When dealing with microwave remote sensing, among the possible choices, the minimum $p-$norm constraint, with $1 < p \leq 2$, allows obtaining reconstructions in Hilbert ($p = 2$) and Banach ($1 < p < 2$) subspaces. Recently, it has been experimentally proven that reconstructions in Banach subspaces mitigate the oversmoothing and the Gibbs oscillations that typically characterize reconstructions in Hilbert subspaces. However, no fair intercomparison among the different reconstructions has been done.

In this study, a mathematical framework to analyze reconstructions in Hilbert and Banach subspaces is provided. The reconstruction problem is formulated as the solution of a $p-$norm constrained minimization problem. Two signals are considered that model abrupt and spot-like discontinuities. The study, undertaken in both the noise-free and the noisy case, demonstrates that l^p reconstructions for $1 < p < 2$ significantly outperform the l^2 ones when spot-like discontinuities are considered; when dealing with abrupt discontinuities, l^2 and l^p reconstructions are characterized by similar performance; however, l^p reconstructions exhibit oscillations when the background is not properly accounted for.

Index Terms

Microwave radiometry, inverse problem.

I. Introduction

A broad class of problems arising in physics or engineering consists of finding a function f such that a known operator L transforms f into a given function b. Basically, L is the so-called forward operator, which represents

F. Lenti is with the Dipartimento di Scienza e Alta Tecnologia, Università degli Studi dell'Insubria, Como, Italy e-mail: flavia.lenti@uninsubria.it

F. Nunziata and M. Migliaccio are with the Dipartimento di Ingegneria, Università degli Studi di Napoli Parthenope, Napoli, Italy e-mail: {ferdinando.nunziata, maurizio.migliaccio} @uniparthenope.it

C. Estatico is with the Dipartimento di Matematica, Università degli Studi di Genova, Genova, Italy e-mail: estatico@dima.unige.it

the known mathematical model, b is the known data and f is the unknown to retrieve. These problems usually belong to the class of inverse problems, such as identification, synthesis, reconstruction, inverse scattering, image restoration, etc., when practical applications, e.g. remote sensing, probing of media, pattern recognition etc. [1]-[21], are considered.

The basic inverse problem arising in microwave applications can be formulated according to a linear integral equation that describes the relationship between the t-th measurement b_t and the unknown function f:

$$b_t = \int_{\Omega} G_t(\mathbf{z}) f(\mathbf{z}) d\mathbf{z}, \tag{1}$$

where $\mathbf{z}$ is the integration variable. In particular eq.(1) is a Fredholm equation of the first kind with a smooth kernel G_t. When a microwave device is considered, G_t is the low-pass system aperture function and, hence, the problem of solving (1), with respect to unknown f, is an ill-posed inverse problem [2]. This implies that even small errors in the data, b_t can produce very large errors in the result, f. Hence, the problem has to be regularized to obtain reasonable approximations of the sought solution.

If the kernel G_t is bandlimited, (1) in discrete setting reads as:

$$b_t = \mathbf{A}_t^T \mathbf{x}, \tag{2}$$

where $\mathbf{A}_t$ is the sampled version of the kernel $G_t(\cdot)$ and $\mathbf{x}$ is the corresponding sampled version of $f(\cdot)$. To estimate $\mathbf{x}$ from m measurements $\mathbf{b} = (b_1, ..., b_m)$, the following linear system is to be solved:

$$\mathbf{b} = A\mathbf{x}, \tag{3}$$

where $A = (\mathbf{A}_1, ..., \mathbf{A}_m)^T$. The matrix A is a mapping from X to Y where $X \subseteq \mathbf{R}^n$ is the domain of A and $Y \subseteq \mathbf{R}^m$ is the codomain. The identification problem, i.e. reconstructing $\mathbf{x}$ from the aperture-filtered samples $\mathbf{b}$, relies on a proper inversion of the mapping A. The mapping is invertible if and only if it is bijective and this property can be satisfied according to the structure of the system that can be full-determined, over-determined and under-determined. For the purpose of this study, the under-determined case will be discussed since it typically applies when dealing with spatial resolution enhancement of microwave remotely sensed measurements, where coarse but partially correlated measurements are exploited to reconstruct the signal on a finer resolution grid. The under-determined system implies that no inverse matrix exists since the mapping is not injective: two elements belonging to X may be mapped in the same element $\mathbf{b} \in Y$. To make the mapping invertible, two subspaces X_s and Y_s must be considered for X and Y, respectively. This allows defining the mapping $A^s : Y_s \rightarrow X_s$ such that $A^s(A\mathbf{x}) = \mathbf{x} \ \ \forall \ \mathbf{x} \ \in X_s$. It must be explicitly pointed out that the functional A^s may be even non-linear. Choosing X_s and Y_s corresponds to select one of the infinite solutions that satisfy the under-determined system. The reconstructed signal lies in X_s; however, this may not be the case for the original signal. Therefore, the reconstructed signal in X_s may not be the closest one to the original one. Choosing X_s and Y_s is equivalent to impose a constraint on the signal to be reconstructed. Since there are different constraints that can be imposed to define the mapping

A^s, there are also different mappings that can produce different reconstructions from the same data. In the frame of spatial resolution enhancement of microwave data, different choices are possible [7]-[21]. Among the possible choices, the minimum $p-$norm, with $1 < p \leq 2$ results in reconstructions spanning from Hilbert ($p = 2$) to Banach ($1 < p < 2$) subspaces. When $p = 2$, the well-known l^2- norm is achieved, which can be physically interpreted as energy. In literature, some methods have been proposed to enhance the spatial resolution of microwave probes based on the minimum l^2- norm constraint. The classical Backus-Gilbert [2], [7] inversion technique is used in [8] as a deconvolution method to enhance low frequency SSM/I measurements. The algebraic reconstruction technique (ART) [2], [9] is used in [10] to enhance the spatial resolution of ERS-2 and SEAWINDS scatterometer data. The truncated singular value decomposition (TSVD) [2] is used in [11] to deal with spatial resolution enhancement of SSM/I one-dimensional data. This technique is extended to actual two-dimensional SSM/I data in [12]. The Landweber method [2] is used in [14] to enhance the spatial resolution of simulated microwave radiometer data. In addition, a faster-convergence Landweber method is proposed that is contrasted with the conventional Landweber and with the ART. The Tikhonov [2] method is used in [13] to enhance the spatial resolution of one-dimensional radiometer measurements.

Usually, the choice of the l^2-norm gives rise to smooth (and sometimes over-smooth) solutions and Gibbs-related oscillations where abrupt discontinuities are present. This is a key problem, for instance, on the boundary between land and ocean both for scatterometer and radiometer measurements. Indeed, the actual raw measurements blur the land/ocean boundary give rise to biased measurements along the coast. This blurring effect is even more noticeable when small islands are present. In fact, due to their small size, the measurements are smeared not only along the coastline but throughout the interiors as well [8].

Recently, to overcome the drawbacks related to the l^2-norm, the resolution enhancement problem has been cast in the Banach subspaces [16]. The rationale relies on the fact that when $p-$norm, with $1 < p < 2$ is used, the oversmoothness and the Gibbs oscillations related to the energy norm are reduced. Experiments, performed on both simulated and actual microwave radiometer data, confirm the soundness of the proposed rationale. In addition, some drawbacks have been pointed out. Among them, the non-linearity of the inverse operator and the key role played by the background in the reconstructions are the most important. Moreover, a fair intercomparison among reconstructions obtained in different subspaces is not straightforward since their performance strongly rely on the specific parameters that characterize the reconstruction algorithm.

In this study, the reconstruction problem is formulated as the solution of a minimum $p-$norm constrained minimization problem in order to let the solution independent on the specific algorithm and to allow a fair intercomparison among the reconstructions obtained in Hilbert and Banach subspaces. To discuss the reconstruction performance, two one-dimensional signal models are considered that emulate abrupt and spot discontinuities and a set of qualitative parameters is introduced both in the spatial and in the Fourier transformed domain.

The study, undertaken in both noise-free and the noisy cases, demonstrates that l^p reconstructions for $1 < p < 2$ significantly outperform the l^2 ones when spot-like discontinuities are considered; when dealing with abrupt discontinuities, l^2 and l^p reconstructions are characterized by similar performance; however, l^p reconstructions exhibit oscillations when the background is not properly accounted for.

The remainder of the paper is organized as follows. In Section II the theoretical framework is reviewed both in the noise-free and noisy case, in Section III the reconstruction performance is discussed, while the conclusions are drawn in Section IV.

II. Theoretical background

In this section, the mathematical background to analyze the properties of the signal reconstructed from an underdetermined system is provided. To make the analysis independent of the specific algorithm, the inverse mapping is formulated as a l^p constrained minimization problem. Two subspaces are considered: the first one that corresponds to choosing the solution resulting in minimum energy, i.e. the l^2-norm is considered; the second one that corresponds to choosing the solution resulting in the minimum l^p norm, with $1 < p < 2$. In addition, noise-free and noisy data are discussed.

A. Noise-free case

In this subsection, the computation in the noise-free case is described.

When the l^2-norm is considered, the following minimization problem is solved:

$$min \parallel \mathbf{x} \parallel_2^2 \text{ subject to } A\mathbf{x} = \mathbf{b}. \tag{4}$$

Since the functional $\parallel \mathbf{x} \parallel_2^2$ is convex it can be demonstrated that $\bar{\mathbf{x}}$ is a global minimum for (4) if and only if there exists $\bar{\boldsymbol{\nu}} \in \mathbf{R}^m$ such that $(\bar{\mathbf{x}}, \bar{\boldsymbol{\nu}})$ satisfies the $(m+n) \times (m+n)$ linear system:

$$\begin{cases} A\bar{\mathbf{x}} &= \mathbf{b} \\ \nabla F(\bar{\mathbf{x}}) - A^*\bar{\boldsymbol{\nu}} &= 0. \end{cases} \tag{5}$$

where $F(\bar{\mathbf{x}}) = \parallel \bar{\mathbf{x}} \parallel_2^2$ so that $\nabla F(\bar{\mathbf{x}}) = \bar{\mathbf{x}}$. Solving the equality constrained convex minimization (5) is equivalent to find the solution of the Kerush-Kuhn-Tucker system (5) (KKT) [22], whose solution is:

$$\begin{cases} \bar{\boldsymbol{\nu}} &= (AA^*)^{-1}\mathbf{b} \\ \bar{\mathbf{x}} &= A^*(AA^*)^{-1}\mathbf{b}. \end{cases} \tag{6}$$

Note that $A^*(AA^*)^{-1} = A^\dagger$ is known as Moore-Penrose pseudo-inverse for an underdetermined system and it is a linear inverse functional.

When the l^p-norm is considered, the following problem is to be solved:

$$min \parallel \mathbf{x} \parallel_p^p \text{ subject to } A\mathbf{x} = \mathbf{b}. \tag{7}$$

where $\| \mathbf{x} \|_p^p = \sum_{i=1}^n |x_i|^p$. The p-norm is the discrete version of the norm of the space L^p, which is the space of the p-power integrable functions. Despite of the l^2 space, the l^p space, for $p \neq 2$, is not a Hilbert space, but is only a Banach space. The latter is a complete normed linear space that is not equipped with any scalar product. This means that in Banach spaces the "angle" between two elements is not defined.

Even in this case, the functional $\| \mathbf{x} \|_p^p$ is convex, therefore a minimization problem can be considered again, which leads to the corresponding KKT system (5) with $F(\bar{\mathbf{x}}) = \| \bar{\mathbf{x}} \|_p^p$ so that $\nabla F(\bar{\mathbf{x}}) = J_p(\bar{\mathbf{x}})$ where $J_p(\bar{\mathbf{x}}) = (J_1, J_2, ..., J_n)$ whose components are $J_i = |x_i|^{p-1} sign(x_i)$ with $sign(x_i)$ is the sign-function. Therefore, differing from the l^2- norm case, a non-linear system is obtained that does not admit a closed form solution. To solve the KKT non-linear system, an extension of the Newton's method that includes equality constraint is used [22], [23]. A $\mathbf{b}-$dependent solution is obtained that, unlike the l^2-case, does not allow defining explicitly the pseudo-inverse operator.

B. Noisy-case

In this subsection, the rationale followed to address the reconstruction in the noisy-case, is described.

The system (3), when noisy measurements are available, becomes:

$$A\mathbf{x} = \mathbf{b}_n, \tag{8}$$

where $\mathbf{b}_n = \mathbf{b} + \mathbf{n}$ with $\mathbf{n} \in \mathbf{R}^m$ whose components are related to the additive white Gaussian noise (AWGN).

This problem represents the discretized version of eq. (1) and, therefore, the matrix A is ill-conditioned. This implies that, to avoid noise amplification, regularization methods must be applied.

Hence, according to the discrepancy principle [2], the constraint that characterizes eq. (4) and (7) must be replaced by the following one:

$$\| A\mathbf{x} - \mathbf{b}_n \|_2^2 \leq c \cdot \varepsilon, \tag{9}$$

where ε is an estimate of the 2-norm of the error , i.e. $\| \mathbf{n} \|_2^2 = \varepsilon$ and $c \geq 1$ rules the trade-off between regularization and noise amplification.

Accordingly, when (9) is used, eq. (4) and (7) become:

$$min \| \mathbf{x} \|_2^2 \ \text{ subject to } \ \| A\mathbf{x} - \mathbf{b}_n \|_2^2 \leq c \cdot \varepsilon, \tag{10}$$

and

$$min \| \mathbf{x} \|_p^p \ \text{ subject to } \ \| A\mathbf{x} - \mathbf{b}_n \|_2^2 \leq c \cdot \varepsilon, \tag{11}$$

respectively. Note that to allow a fair intercomparison, the constraint (9) is used in both Hilbert (10) and Banach (11) subspaces. The problems (10) and (11) are inequality constrained convex problems whose solutions can be

obtained by solving the KKT system [22]:

$$\begin{cases} \nabla f(\bar{\mathbf{x}}) + \mu \nabla g(\bar{\mathbf{x}}) = 0 \\ g(\bar{\mathbf{x}}) \leq 0 \\ \mu \geq 0 \\ \mu g(\bar{\mathbf{x}}) = 0, \end{cases} \tag{12}$$

where $f(\mathbf{x}) = \| \mathbf{x} \|_2^2$ and $f(\mathbf{x}) = \| \mathbf{x} \|_p^p$ when (10) and (11) is adopted, respectively, and $g(\mathbf{x}) = \| A\mathbf{x} - \mathbf{b}_n \|_2^2 - c \cdot \varepsilon$. In our approach, to solve the KKT system, the interior-point method, that applies the Newton's method to a sequence of equality constrained problems, is used [22], [23].

III. Analysis of reconstructions in Hilbert and Banach subspaces

In this study, the performance of the reconstructions is analyzed in Hilbert and Banach subspaces and in both the noise-free and noisy cases with reference to an underdetermined system resulting from a spatial resolution enhancement problem.

To fully characterize the problem (3), the $A \in \mathbf{R}^{m \times n}$ matrix and the measurements vector $\mathbf{b} \in \mathbf{R}^m$ are needed.

A realistic one-dimensional microwave remote sensing system that performs $m = 64$ uniformly spaced and partially overlapped measurements is considered, see "grid 1" in Fig.1. The system aperture function is given by a shift-invariant Gaussian-shaped function, $G(\cdot)$, whose 3 dB width is equal to 69 samples.

To perform spatial resolution enhancement, the unknown function is to be reconstructed using a finer grid. In this study, $n = 1400$ uniformly spaced samples are considered, see "grid 2" in Fig.1. Hence, the $i-$th row of the A matrix is given by the sampled and shifted version of the aperture function:

$$G(z - ir), \tag{13}$$

where $y = (z - ir) \in [1 : 1400]$ and $r = \frac{n}{m}$.

To obtain the measurements vector **b**, eq.(3) is used where **x** is obtained sampling a reference signal model. Since, in this study, we want to model abrupt and spot discontinuities, a rect signal model is considered:

$$f(y) = a \text{ rect}\left(\frac{y - y_1}{\Delta}\right), \tag{14}$$

where $a = 100$ and $\text{rect}(t) = \begin{cases} 1 & |t| < 1 \\ 0 & |t| > 1 \end{cases}$.

The two signal models are:

- $f_1(y) = \begin{cases} y_1 = 500 \\ \Delta = 300 \end{cases}$,
- $f_2(y) = \begin{cases} y_1 = 410 \\ \Delta = 10 \end{cases}$.

Those signal models represent abrupt discontinuities ($f_1(y)$), e.g. the land-sea interface observed by a microwave radiometer/scatterometer, and spot discontinuities ($f_2(y)$), e.g. small islands and lakes observed by a microwave radiometer/scatterometer.

To discuss the experiments in a more quantitative way, five key parameters ($co,\ h_n,\ \gamma_1,\ \gamma_2,\ W$) are introduced to analyze the performance of the reconstructions.

co is the correlation coefficient between the reference signal and the reconstructed one. h_n deals with the performance in reconstructing correctly the amplitude level and it is given by the ratio between the mean value of the non-zero signal level and the signal amplitude a. γ_1 and γ_2 deal with the broadening of the reconstructed signal with respect to the reference one. In particular, γ_1 is the angle between $\overline{S_1S_2}$ and $\overline{S_1S_3}$, see Fig.2, where S_1 is the intersection between the leading edge of the reference signal and measurements; S_2 is the first point (i, b_i) such that $b_i = a$; $S_3 = (y_1 - \Delta, a)$. γ_2 is the angle between $\overline{S_1S_4}$ and $\overline{S_1S_5}$, see Fig.2, where S_4 is the last point (i, b_i) such that $b_i = 0$ and $i < y_1 - \Delta$; $S_5 = (y_1 - \Delta, 0)$. W is a parameter that relates the widths of the Fourier transformed reference and measured signals. This parameter will be fully described in the subsequent experiments.

To clarify the expected behavior of the parameters, two extremes must be identified. The first one is obtained when the reference signal is considered. In this case, the reference values are achieved for the five parameters, i.e. $co = 1,\ h_n = 1,\ \gamma_1 = \gamma_2 = 0$ and $W = 1$. The second one is obtained when the measured signal (to obtain the same size of the reference signal, the approach proposed in [20] is used, i.e. the value of the nearest measurements is assigned to each pixel) is considered. In this case, the low-pass nature of the kernel that describes the measurement system, results in a measured signal: a) broader that the reference one, i.e. $\gamma_1 > 0$ and $\gamma_2 > 0$ is expected; b) characterized by an amplitude level attenuated with respect to the reference signal, i.e. $h_n < 1$ is expected. As a matter of fact, $co < 1$ and $W > 1$ are also to be expected.

When dealing with reconstructed signals, intermediate values are expected. The closer are the values to the reference ones, the better is the reconstruction.

To characterize the errors inherently related to the reconstructions two additional parameters are introduced ($d1$ and $d2$). Both the parameters, which will be fully described in the subsequent experiments, measure the oscillations that characterize the reconstructed signals.

A. Noise-free case

The first experiment consists of analyzing the signal $\mathbf{x}_1$ (see Fig.2) reconstructed at enhanced spatial resolution both in Hilbert (l^2) and Banach (l^p with $1 < p < 2$) subspaces. In this study, following the theoretical and experimental rationale developed in [16], the Banach subspaces defined by $p = 1.8,\ 1.5$ and 1.2 are considered.

The measurements, see cyan points in Fig.2, are a smoothed version of the reference signal. The values of $co,\ h_n,\ \gamma_1$ and γ_2 are equal to $0.97,\ 1,\ 49^o$ and 30^o, respectively, see Table I.

The signal, reconstructed at enhanced resolution in the l^2 subspace, is shown in Fig.3(a), see red x-mark. Note

also that, to better analyze the reconstructions, only the range $[0, 500]$ samples is shown. The reconstructed signal well fits the reference one and the abrupt discontinuity is well reconstructed. In fact, h_n is close to 1 and the γ_1 and γ_2 angles are equal to 19.3^o and 14.1^o, respectively (see Table I). Hence, they are significantly reduced with respect to the ones related to the measurements of Fig.2. It can be noted that Gibbs oscillations are present. The maximum amplitude of these oscillations, as expected, occurs near the upper and the bottom part of the discontinuity and its value, normalized to a and evaluated at the upper ($d1$) and lower ($d2$) part of the discontinuity, is equal to 8% and 8%, respectively, (see Table I). Note that, as expected, similar numbers apply for the discontinuity on the right-hand side of the Fig.3 (not shown to save space).

The correlation coefficient is equal to 0.99 and demonstrates that a high-quality reconstruction is obtained. To analyze reconstruction performance in the Fourier domain, the reference signal and the l^2 reconstructed one are Fourier transformed in Fig.3(b). The Fourier signals are shown in the range $[924, 1124]$ and are properly scaled to allow an easier comparison. It can be noted that the reconstructed signal is equal to the reference one over the range labeled as R1 while differences are exhibited at higher frequencies over the range R2. The Fourier transform of the reconstructed signal becomes negligible over the range R3; this justifies Gibbs oscillations that characterize the reconstructed signal in Fig.3(a).

To quantify the enhancement of the spatial resolution of the reconstructed signal, the relationship between the reference and the reconstructed signal is needed. One can consider $\mathbf{x}$ and $\mathbf{x}_{rec}$ as the input and the output of an equivalent system given by the cascade of two systems. The first one is a linear operator that rules the transformation of the reference signal into the measurements ($A\mathbf{x} = \mathbf{b}$). The second one is a linear operator that rules the transformation of the measurements into the reconstructed signal ($\mathbf{x}_{rec} = A^{\dagger}\mathbf{b}$), see Fig.4. Hence, for the signal $\mathbf{x}_1$, $\mathbf{x}_{rec}$ is given by:

$$\mathbf{x}_{rec} = A^{\dagger}A\mathbf{x}_1 = C\mathbf{x}_1, \tag{15}$$

where C is a $n \times n$ matrix whose $i-th$ row represents the point spreading function (PSF) of the $i-th$ point. To quantify the obtained spatial resolution, the 3 dB width of the $i-th$ PSF is measured. The spatial resolution varies between 24 and 27 samples and the minimum is reached when approaching points of "grid 1", see Fig.2.

The signals reconstructed at enhanced resolution in the l^p subspaces with $p = 1.8,\ 1.5$ and 1.2 are shown in Fig.3(a). Note that in all the subsequent experiments, we denote Hilbert and Banach subspaces with "l^2" and "l^p", respectively. The reconstructed signals fit well the reference signal and the abrupt discontinuity is well reconstructed. To compare the reconstruction accuracy, h_n, γ_1, γ_2, co, $d1$ and $d2$ are reported in Table I. The angles γ_1 and γ_2 measured in l^p are always smaller than the correspondent l^2 ones ($19.3^o,\ 14.1^o$). This shows that the Banach subspaces allow a better reconstruction of the abrupt discontinuity with respect to the l^2 subspace. Moreover, the reconstruction accuracy increases for decreasing p and it achieves the best performance ($11.7^o,\ 9.3^o$) at $p = 1.2$. A different behavior is obtained for $d1$ and $d2$. The latter one, see Table I and Fig.3(a), is always smaller than the

correspondent $p = 2$ one (8%) and it decreases for decreasing p, showing that negligible oscillations are obtained at $p = 1.2$ (0.5%). An opposite behavior characterizes $d1$, which is always larger than the correspondent $p = 2$ one (8%) and it increases for decreasing p. The maximum amplitude of the oscillations is exhibited at $p = 1.2$ (14%). This behavior shows that the background level plays a key role when reconstruction is addressed in Banach subspaces. In fact, in Banach subspaces with small parameter p a lower penalty term $\| \mathbf{x} \|_p$ is associated to elements with large but few components and a higher penalty is associated to elements with many but small components. This justifies the smallest (largest) oscillations resulting from the $l^{1.2}$ reconstruction when the background is 0 (100). It can be noted that even in Banach subspaces, a high-quality reconstruction is obtained ($co = 0.99$).

The Fourier transforms of the l^p reconstructed signals are shown in Fig.3(b). As far as for the l^2 case, even in l^p the reconstructed signals are equal to the reference one in R1 while showing some differences in R2. The difference between l^2 and l^p is observed in R2 where l^p subspaces allow reconstructing the signal even in R2. This justifies the reduction of Gibbs oscillations obtained for decreasing p. However, the transformed reconstructed signals do not well fit $\mathbf{x}_1$ in R2. Note that in $R3$ all the transformed signals vanish.

To analyze the resolution enhancement capability obtained in the l^p subspaces, the approach followed in l^2 cannot be adopted since the functional A^s is now not linear, i.e. depends on the input signal. Hence, the PSF cannot be defined straightforwardly for a non-linear system. We consider that the latter, when linearized around a point, is slowly variant. Therefore, given a certain input/output relationship that characterizes the non-linear system, one can found an equivalent linear and shift-invariant system whose input/output relationship approximates the non-linear one [21]. Hence, the Fourier transform of the equivalent transfer function ($F(ETF)$) of the non-linear system is given, for $|F(\mathbf{x}_1)| \neq 0$:

$$F(ETF) = \frac{F(\mathbf{x}_{rec})}{F(\mathbf{x}_1)}, \tag{16}$$

where F stands for Fourier transform. A measure of the spatial resolution is given by the width of the absolute value of the correlation function, R, measured as the inverse Fourier transform of the spectrum [21]:

$$R = |F^{-1}\left(F(ETF)F(ETF)^*\right)|, \tag{17}$$

where $|\cdot|$ stands for absolute value and F^{-1} is the inverse Fourier transform. Note that when the reconstructed signal tends to the reference one, the R function tends to a Dirac delta function.

To allow a fair comparison of the spatial resolution enhancement achieved in Banach and in Hilbert subspaces, the above-mentioned approach is applied also for $p = 2$ and for the measurements. The R function is shown for $p = 1.2,\ 1.5,\ 1.8,\ 2$ in Fig.5. It can be noted that, for decreasing p, the height of the R functions increases while its width decreases witnessing that the spatial resolution gets finer for decreasing p.

To quantify the spatial resolution enhancement, the parameter W, given by the 3 dB width of the R function, is evaluated. In this case, $W = 38,\ 37,\ 36$ and 32 for $p = 2,\ 1.8,\ 1.5$ and 1.2, respectively and $W = 67$ for

the measurements (see Table I). This confirms that the spatial resolution is enhanced. A finer spatial resolution is achieved for decreasing p and the best performance, i.e. the finest spatial resolution, is achieved at $p = 1.2$.

For sake of completeness $p < 1.2$ is also considered. In particular, the reconstruction performance relevant to the cases $p = 1.1$ and $p = 1.05$ is discussed in Table I. It can be noted that the trend observed in the previously discussed Banach spaces is confirmed. Hence, as far as for the previous cases, all the parameters improve but $d1$. It must be explicitly noted that, although reconstruction performance improves at descending p, given that $p > 1$, this is contrasted by algorithm instability. Hence, the best compromise is achieved at $p = 1.2$ [16]. The limit case of Banach space corresponding to $p = 1$ dramatically fails in the reconstruction, since the reference signal is not sparse enough.

The second experiment consists of analyzing the signal $\mathbf{x}_2$ (see Fig.6) reconstructed at enhanced resolution in Hilbert and Banach subspaces. The measurements, see cyan points in Fig.6, are a smoothed version of the original signal $\mathbf{x}_2$. Note that, in this case, the original signal can hardly be visually recognized from its smoothed version. This smoothing can be quantitatively measured by the objective parameters defined in the previous experiment. Note that, since in this experiment the reference signal is significantly smoothed by the measurements system, γ_1 is re-defined using a different point S_2. In fact, $S2$ is given by the coordinates of the maximum of $\mathbf{b}$. In detail, $\gamma_1,\ \gamma_2,\ h_n$ and co are equal to $80^o,\ 16.3^o,\ 0.26$, and 0.54 respectively (see Table II). This witnesses that this experiment is by far more challenging than the previous one. The values of the parameters show that here the measured signal is significantly different from the reference one, see the small co value (0.54) in Table II, which shows that there is a low correlation between the reference signal and the measurements. Moreover, in this case, measurements are slightly shifted with respect to the reference signal, see Fig.6.

The signal reconstructed at enhanced resolution in the l^2 subspace is shown in Fig.7(a), see red x-mark. The reconstructed signal fits enough the reference signal. In fact, the co parameter is equal to 0.79. The abrupt discontinuity is recovered, as it is shown by the γ_1 and γ_2 angles that are equal to 45.0^o and 15.3^o, respectively (see Table II). Hence, they are significantly reduced with respect to the ones related to the measurements of Fig.6. The h_n value witnesses that the reconstructed signal amplitude is about 65% of the original one; moreover, Gibbs oscillations are present that result in $d2$ value equal to 11%, see Table II. Note that the parameter $d1$ is not measured.

The reference signal and the l^2 reconstructed one are Fourier transformed, see Fig.7(b). To better visualize the output, transformed signals are restricted to the range $[724, 1324]$. It can be noted that, also in this case, the Fourier transform of the reconstructed signal is equal to the Fourier transform of the reference one over the range labeled as R1 in Fig.7(b). Differences apply at higher frequencies over the range R2, see Fig.7(b). The Fourier transform of the reconstructed signal vanishes over the range R3; this justifies Gibbs oscillations that characterize the reconstructed signal in Fig.7(a) and the failure in reconstructing correctly the signal level.

The signal reconstructed at enhanced resolution in the l^p subspaces with $p = 1.8,\ 1.5$ and 1.2 is shown in Fig.7(a). The reconstructed signals well fit the reference signal and the abrupt discontinuity is well reconstructed. To quantify the reconstruction accuracy, γ_1, γ_2, $h_n,\ d2$ and co are measured, see Table II. Even in this case, as far as for the previous experiment, the Banach subspaces provide a better reconstruction of the abrupt discontinuity. In fact, γ_1 and γ_2 are always smaller than the correspondent l^2 ones (45.0^o and 15.3^o). Their value decreases for decreasing p and the minimum value (10.6^o and 6.9^o) is achieved at $p = 1.2$. $d2$ decreases for decreasing p becoming negligible at $p = 1.2$ (1%). In addition, one can note that, unlike the l^2 case, in the l^p subspaces the signal level is better reconstructed, see h_n in Table II. In fact, h_n is always larger that the correspondent l^2 one and gets closer to one for decreasing p. The best performance is obtained at $p = 1.2$ ($h_n = 1.04$), witnessing that at $p = 1.2$ the signal level is well-reconstructed. With respect to the correlation coefficient, it can be noted that even in this case Banach subspaces allow the best reconstruction performance, see co in Table II. However, unlike the previous experiment where all the Banach subspaces resulted in the same co value, here co value increases for decreasing p, reaching the maximum ($co = 0.94$) at $p = 1.2$. This analysis confirms that the best reconstruction performance is achieved at $p = 1.2$.

The Fourier transform of the l^p reconstructed signals is shown in Fig.7(b). As far as for the l^2 case, even in l^p the transformed reconstructed signals are equal to the transformed reference one in R1 while showing some differences in R2. The difference between l^2 and l^p is observed in R3 where the l^p subspaces allow reconstructing the signal even in R2 leading to a reduction of Gibbs oscillations for decreasing p. Note that, even in this case, all the transformed signals vanish in R3.

Moreover, it can be noted that for decreasing p, the Fourier transform of the reconstructed signals better fits the main lobe of $F(\mathbf{x}_2)$. This justifies the best reconstruction of the reference signal provided by $l^{1.2}$.

The R function (17) is shown in Fig.8 for both Hilbert and Banach subspaces. As far as for the previous experiment, for decreasing p, the height of R increases and its width decreases. To quantify the resolution enhancement capability, the same approach, used in the previous experiment, is adopted. In this case, W is equal to $38,\ 36,\ 22$ and 14 for $p = 2,\ 1.8,\ 1.5$ and 1.2, respectively. Hence, the spatial resolution gets finer for decreasing p. It can be noted that, due to the linearity of the l^2 functional, both in the previous and in this experiment the same spatial resolution is achieved, i.e. $W = 38$. Moreover, in the previous experiment W decreased from 37 down to 32 for $p = 1.8$ down to $p = 1.2$. In this experiment, a stronger reduction is obtained since W decreases from 36 down to 14 for $p = 1.8$ down to $p = 1.2$. This implies that when spot signals are considered the reconstruction undertaken in Banach subspaces significantly outperforms the Hilbert one.

Even in this case, the Banach spaces $p = 1.1$ and $p = 1.05$ are discussed in Table II. It can be noted that the reconstruction performance is similar to the one obtained using $p = 1.2$ but for the parameters h_n and $d2$. The former one is significantly larger than the $p = 1.2$ one, witnessing that the signal amplitude is badly reconstructed.

$d2$ is smaller than the $p = 1.2$ one, witnessing that practically negligible Gibbs oscillations are present.
Even in this case the reconstruction fails in the Banach space $p = 1$, since the signal model is only almost sparse [15]. According to [15], when an almost sparse signal is considered, $p > 1$ performs better than $p = 1$.

B. Noisy-case

To analyze reconstruction performance in the noisy case, Monte Carlo simulation is used that consists of applying several noise realizations to the measurements resulting from the two reference signals.
The noise follows a zero-mean Gaussian distribution whose standard deviation is 10%. Note that this is a realistic noise level that, for instance, is typically used when analyzing microwave radiometer [16]. For each noisy measurement, the signal is reconstructed both in Hilbert (10) and in Banach (11) subspaces. Finally, the mean and the standard deviation of the parameters, introduced in the noise-free case, are evaluated. In addition, to analyze the trade-off between regularization and noise amplification, two c values ($c = 1$ and $c = 2$) are considered in the discrepancy principle (9). The former corresponds to use the estimate of the 2-norm of the error; while $c = 2$ implies that more regularization is introduced.
After the previous noise-free experiments, now the third experiment addresses reconstruction performance in Hilbert and Banach subspaces using noisy measurements related to the signal $\mathbf{x}_1$ (see Fig. 2). The mean and the standard deviation of the parameters evaluated for both the measurements and the reconstructed signals are listed in Table III, for both $c = 1$ and $c = 2$.
It can be noted that noise affects the measurements that result in a non-zero value of both $d1$ and $d2$. The parameters evaluated considering the reconstructions in Hilbert and Banach subspaces demonstrate that the reconstructions are robust with respect to the noise, since they exhibit a trend similar to the noise-free cases.
Even in this noisy case, γ_1 and γ_2 decrease for decreasing p; while $d1$ ($d2$) increases (decreases) for decreasing p. In addition, the achieved spatial resolution gets finer for decreasing p, indeed the parameter W, when $c = 2$ is used, is equal to $51,\ 50,\ 45$ and 37 for $p = 2,\ 1.8,\ 1.5$ and 1.2, respectively. The significant reduction of the W parameter at $p = 1.2$ comes at a cost in terms of reconstructed signal noise level.
It can be noted that the standard deviation of all the parameters increases for decreasing p. It means that, for smaller p, the result is more dependent on the noise realization. A large co value applies both in Hilbert and in Banach subspaces witnessing that a high-quality reconstruction is obtained.
Results, obtained using $c = 2$ (see Table III), show that, when this signal model is considered, the difference between $c = 1$ and $c = 2$ is negligible.
With respect to the reconstructions obtained using $p < 1.2$ (not shown), it a trend similar to the noise-free cases is obtained. Hence, hereinafter those cases are not furthered.

The fourth experiment addresses reconstruction performance in Hilbert and in Banach subspaces using noisy measurements related to the spot signal $\mathbf{x}_2$ (see Fig.6).

The mean and the standard deviation of the parameters evaluated for both the measurements and the reconstructed signals are listed in Table IV for both $c = 1$ and $c = 2$.

It can be noted that the noise affects the measurements that result in a non-zero $d2$. The parameters, evaluated considering the reconstructions in Hilbert and in Banach subspaces, demonstrate that, also in this case, reconstructions are robust with respect to the noise, since again they exhibit a trend similar to the noise-free ones. The parameters γ_1 and γ_2 show that, even in this case, a remarkable reconstruction of the abrupt discontinuities is achieved when decreasing p. In fact, γ_1 and γ_2 values related to the l^p reconstructions are always smaller than the l^2 ones. The best performance is obtained at $p = 1.2$ (27.5^o and 12.3^o). These numbers, although larger than the correspondent noise-free ones (see Table II), demonstrate that the $l^{1.2}$ subspace provides the best reconstruction even in the noisy case. Similar comments apply for $d2$ that shows that negligible oscillations are obtained for $p = 1.2$. Note also that $d2$ values are significantly smaller than the noise-free ones; this is due to the fact that regularization leads to smooth solution. The co values demonstrate that valuable reconstruction performance is obtained in all the cases. W decreases for decreasing p, witnessing that the finest spatial resolution is obtained when $p = 1.2$.

It is important to remark that, as far as for the noise-free case, when spot-like discontinuities are considered, the reconstruction undertaken in the $l^{1.2}$ significantly outperforms the reconstructions obtained in all the other subspaces.

IV. Conclusions

In this study, the properties of the signal reconstructed in Hilbert and Banach subspaces are analyzed. A common theoretical framework is used to address the reconstruction as a constraint minimization problem and, therefore, to allow a fair intercomparison of the reconstructions performance independently of the specific reconstruction algorithm.

A measurement system that mimics an actual microwave remote sensing probe is used and two reference signal models, which account for abrupt and spot-like discontinuities, are considered to analyze the reconstruction performance in the two subspaces and both in the noise-free and noisy cases. The main outcomes of this study can be summarized as follows:

- When the noise-free case is considered:
  - All the l^p reconstructions with $1 < p \leq 2$ result in good performance.
  - When the abrupt discontinuity is considered, the reconstruction performance slightly improves at descending p, given that $p > 1$. However, reconstructions undertaken in Banach subspaces exhibit additional oscillations when the background is not properly accounted for.
  - When the spot-like discontinuity is considered, the reconstructions obtained in Banach subspaces are significantly better than the correspondent Hilbert one.
- When the noisy case is considered:

  - The reconstruction performance degrades in all the subspaces.
  - When the abrupt discontinuity is considered, the reconstruction performance slightly improves at descending p, given that $p > 1$. The significant reduction of the W parameter at $p \leq 1.2$ is fictitious since it accounts for noise and oscillations too.
  - When the spot-like discontinuity is considered, the reconstruction performance significantly improves at descending p, given that $p > 1$.
- Although reconstructions performance improves when $1 < p < 1.2$, this is contrasted by algorithm instability. Hence, the best compromise is achieved at $p = 1.2$.
- The Banach space $p = 1$ dramatically fails in the reconstructions since both the reference signals are not sparse enough.

REFERENCES

[1] G.A. Deshamps and H.S. Cabayan, "Antenna synthesis and solution of inverse problems by regularization methods," *IEEE Trans. Antennas Propagat.*, vol. AP-20, no. 3, pp. 268-274, 1972.

[2] P.C. Hansen, *Rank-deficient and discrete ill-posed problem: numerical aspects of linear inversion*. Philadelphia: SIAM, ch. 6-7, pp. 132-208.

[3] D. Schiavulli, F. Nunziata, G. Pugliano, M. Migliaccio, "Reconstruction of the normalized radar cross section field from GNSS-R delay-doppler map," *IEEE J. Sel. Topics in Appl. Earth Observ. and Remote Sens.*, vol. 7, no. 5, pp. 1573-1583, 2014.

[4] D. Schiavulli, F. Lenti, F. Nunziata, G. Pugliano, M. Migliaccio, "Landweber method in Hilbert and Banach spaces to reconstruct the NRCS field from GNSS-R measurements," *Int. J. Remote Sens.*, vol. 35, no. 10, pp. 3782-3796, 2014.

[5] C. Estatico, M. Pastorino, and A. Randazzo, "A novel microwave approach based on regularization in Lp Banach spaces," *IEEE Trans. Antennas Propag.*, vol. 60, pp. 3373-3381, 2012.

[6] M. Hanke and M. Bruhl, "Recent progress in electrical impendance tomography," *Inverse problems*, vol. 19, pp. 1-26, 2003.

[7] G.E. Backus and J.F. Gilbert, "Numerical applications of a formalism for geophysical inverse problem," *Geophys. J.R. Astr. Soc.*, vol. 13, pp. 247-276, 1967.

[8] M.R. Farrar and E.A. Smith, "Spatial resolution enhancement of terrestrial features using deconvolved SSM/I microwave brightness temperature," *IEEE Geosci. Remote Sens. Lett.*, vol. 30, no. 2, pp. 349-355, 1992.

[9] Y. Censor, "Finite series-expansion reconstruction methods," *Proc. IEEE*, vol. 71, no. 3, pp. 409-419, 1983.

[10] D.S. Early and D.G. Long, "Image reconstruction and enhanced resolution imaging from irregular samples," *IEEE Trans. Geosci. Remote Sens.*, vol. 39, no. 2, pp. 291-302, 2001.

[11] M. Migliaccio and A. Gambardella, "Microwave radiometer spatial resolution enhancement," *IEEE Trans. Geosci. Remote Sens.*, vol. 4, no. 5, pp. 1159-1169, 2005.

[12] F. Lenti, F. Nunziata, M. Migliaccio, and G. Rodriguez, "Two-dimensional TSVD to enhance the spatial resolution of radiometer data," *IEEE Trans. Geosci. Remote Sens.*, vol. 52, n. 5, pp. 2450-2458, 2014.

[13] A. Gambardella and M. Migliaccio, "On the superresolution of microwave scanning radiometer measurements," *IEEE Geosci. Remote Sens. Lett.*, vol. 5, no. 4, pp. 796-800, 2008.

[14] F. Lenti, F. Nunziata, C. Estatico, M. Migliaccio, "Spatial resolution enhancement of Earth observation products using an acceleration technique for iterative methods," *IEEE Geosci. Remote Sens. Lett.*, vol. 12, no. 2, pp. 269-273, 2015.

[15] T. Schuster, B. Kaltenbacher, B. Hofmann, K.S. Kazimierski, *Regularization methods in Banach spaces*, Radon Series on Computational and Applied Mathematics, 2012.

[16] F. Lenti, F. Nunziata, C. Estatico, and M. Migliaccio, "On the spatial resolution enhancement of microwave radiometer data in Banach spaces," *IEEE Trans. Geosci. Remote Sens.*, vol. 52, n. 3, pp. 1834-1842, 2014.

[17] D.G. Long, P.J. Hardin, P.T. Whiting, "Resolution enhancement of spaceborne scatterometer data," *IEEE Trans. Geosci. Remote Sens.*, vol. 31, n. 3, pp. 700-715, 1993.

[18] D.G. Long, D.L. Daum, "Spatial resolution enhancement of SSM/I data," *IEEE Trans. Geosci. Remote Sens.*, vol. 36, n. 2, pp. 407-417, 1998.

[19] B.A. Williams and D.G. Long, "Reconstruction from aperture-filtered samples with application to scatterometer image reconstruction," *IEEE Trans. Geosci. Remote Sens.*, vol. 49, no. 5, pp. 1663-1675, 2011.

[20] D.G. Long, "Reconstruction and resolution enhancement techniques for microwave sensors," in *Frontiers of remote sensing information processing*, C.H.Chen, World Scientific, ch.11, 2003.

[21] B.A. Williams, "Signal processing methods for ultra high resolution scatterometry," Ph.D. dissertation, Brigham Young Univ., Provo, UT, 2010.

[22] M. Grant and S. Boyd, "CVX: Matlab Software for disciplined convex programming, version 2.0 beta", [Online]. Available: http://cvxr.com/cvx.

[23] M. Grant and S. Boyd, "Graph implementation for nonsmooth convex programs, Recent advances in learning and control", V. Blondel, S. Boyd and K. Kimura editors, pp. 95-110, Springer, 2008.

[24] M. Fornasier and H. Rauhut, "Compressive Sensing," in *Handbook of mathematical methods in imaging*, Springer, pp. 187-228, 2011.

TABLE I

PARAMETERS RELATED TO THE FIRST EXPERIMENT.

	measurements	x_{rec} in l^2	x_{rec} in $l^{1.8}$	x_{rec} in $l^{1.5}$	x_{rec} in $l^{1.2}$	x_{rec} in $l^{1.1}$	x_{rec} in $l^{1.05}$
h_n	1	1.0014	1.0016	1.0017	1.002	1.001	1.001
γ_1	49^o	19.3^o	17.6^o	14.6^o	11.7^o	10.7^o	8.8^o
γ_2	30^o	14.1^o	12.4^o	10.9^o	9.3^o	8.8^o	7.4^o
$d1$	0%	8%	9%	11%	14%	16%	17%
$d2$	0%	8%	6%	3%	0.5%	0.2%	0.08%
co	0.97	0.99	0.99	0.99	0.99	0.99	0.99
W	67	38	37	36	32	30	28

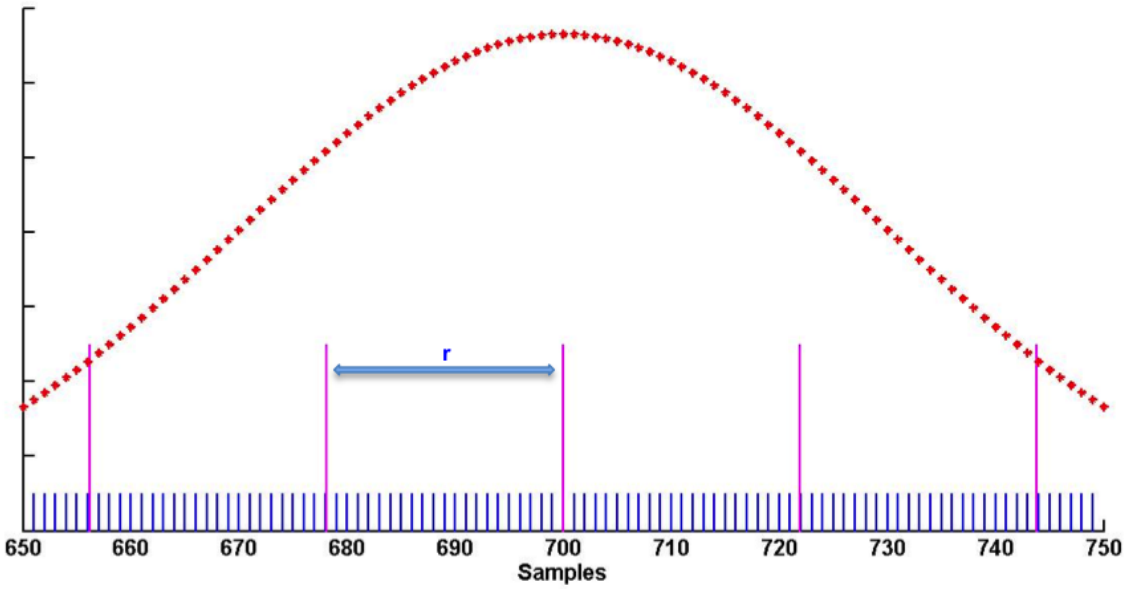

Fig. 1. Sketch of the two sampling grids used in this study (restricted to the range 650-750 samples). "grid 1" is the sampling grid used to simulate the measurement system, which performs $m = 64$ measurements, see magenta vertical lines. "grid 2" is the $n = 1400$ samples grid used to reconstruct the signal at finer spatial resolution, see blue vertical lines. Note that the reference antenna pattern $G(z - ir)$, which in this figure is centered in $i = 32$, is sampled using "grid 2" (see dotted red line).

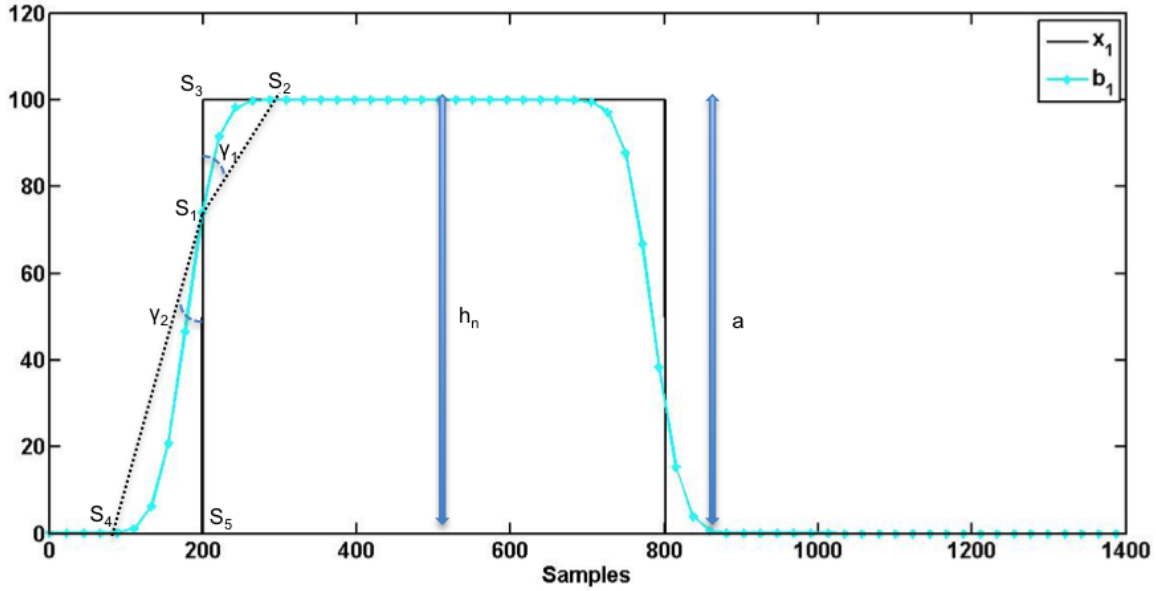

Fig. 2. Reference signal $\mathbf{x}_1$ (continuous black line) and simulated measurements (dotted cyan line).

TABLE II

PARAMETERS RELATED TO THE SECOND EXPERIMENT.

	measurements	x_{rec} in l^2	x_{rec} in $l^{1.8}$	x_{rec} in $l^{1.5}$	x_{rec} in $l^{1.2}$	x_{rec} in $l^{1.1}$	x_{rec} in $l^{1.05}$
h_n	0.26	0.65	0.69	0.81	1.04	1.32	1.34
γ_1	80^o	45.0^o	37.2^o	23.6^o	10.6^o	10.5^o	10.4^o
γ_2	16.3^o	15.3^o	14.1^o	10.0^o	6.9^o	6.6^o	6.4^o
$d1$	–	–	–	–	–	–	–
$d2$	0%	11%	9%	5%	1%	0.5%	0.3%
co	0.54	0.79	0.83	0.89	0.94	0.93	0.93
W	67	38	36	22	14	14	14

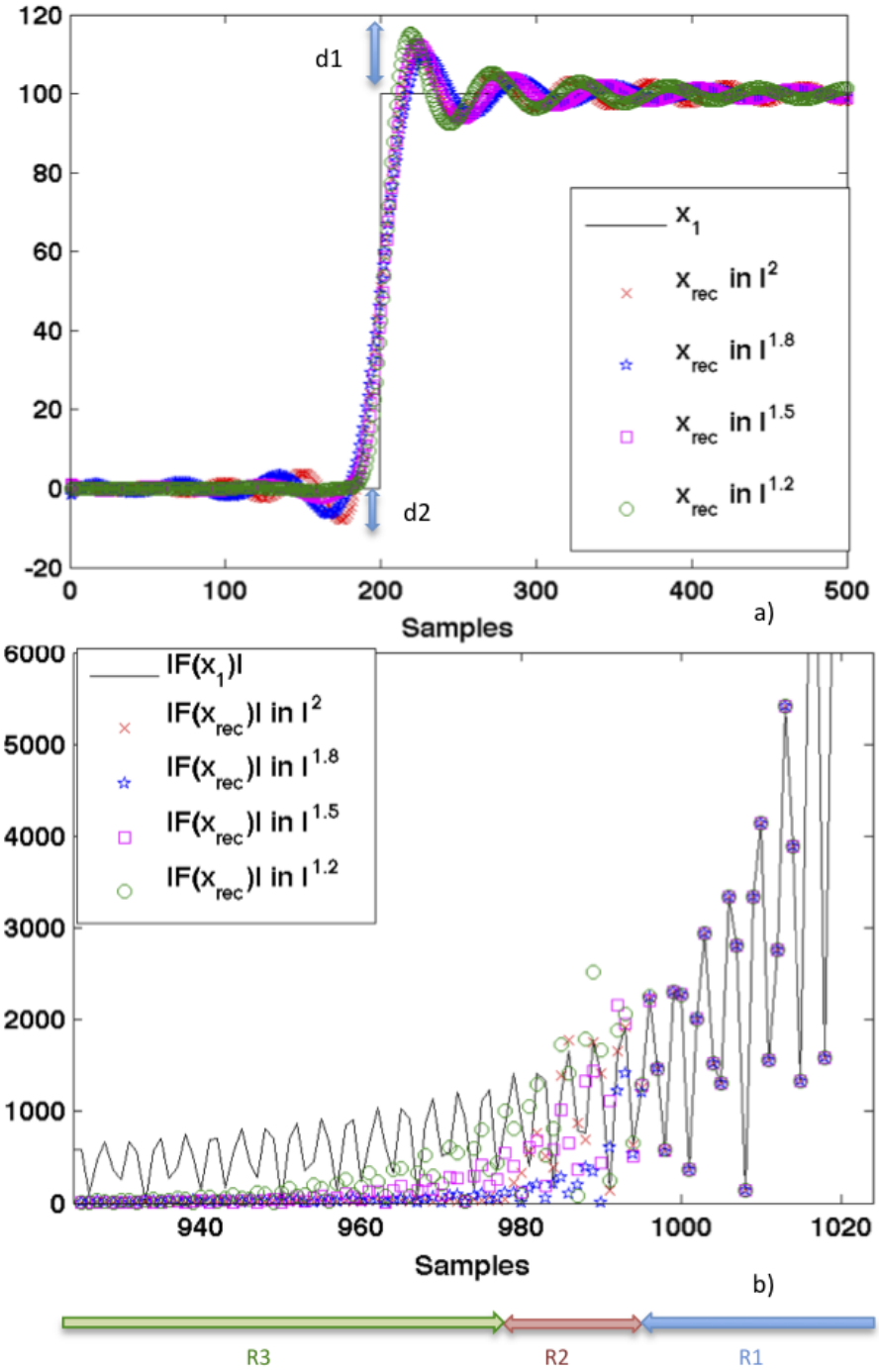

Fig. 3. (a) Reference signal (black line) and reconstructed signal in l^2 subspace (red x-mark) and in l^p subspaces with $p = 1.8$ (blue star), $p = 1.5$ (magenta square) and $p = 1.2$ (green circle), shown in the range $[0, 500]$ samples. (b) Reference signal (black lines) and reconstructed signal in l^2 subspace (red x-mark) and in l^p subspaces with $p = 1.8$ (blue star), $p = 1.5$ (magenta square) and $p = 1.2$ (green circle) in the Fourier domain. Note that R1, R2 and R3 refer to the range $[998 : 1024]$, $[977 : 997]$ and $[1 : 976]$, respectively.

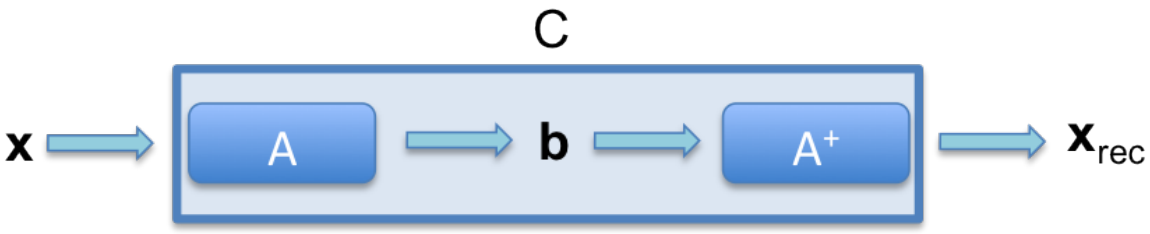

Fig. 4. Sketch of the linear system that rules the transformation of $\mathbf{x}$ into $\mathbf{x}_{rec}$. The system is given by the cascade of two sub-systems related to direct ($A\mathbf{x} = \mathbf{b}$) and the reconstruction($A^{\dagger}\mathbf{b} = \mathbf{x}_{rec}$) problem

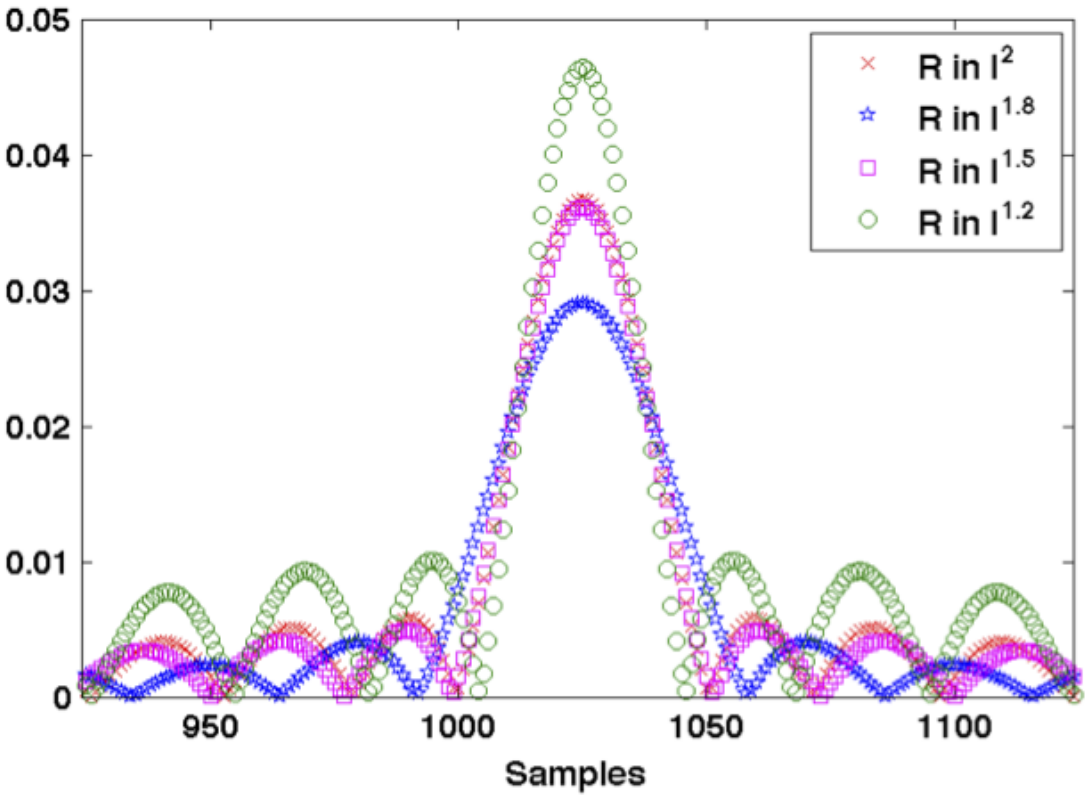

Fig. 5. The R function for $p = 2$ (red x-mark), $p = 1.8$ (blue star), 1.5 (magenta square) and 1.2 (green circle).

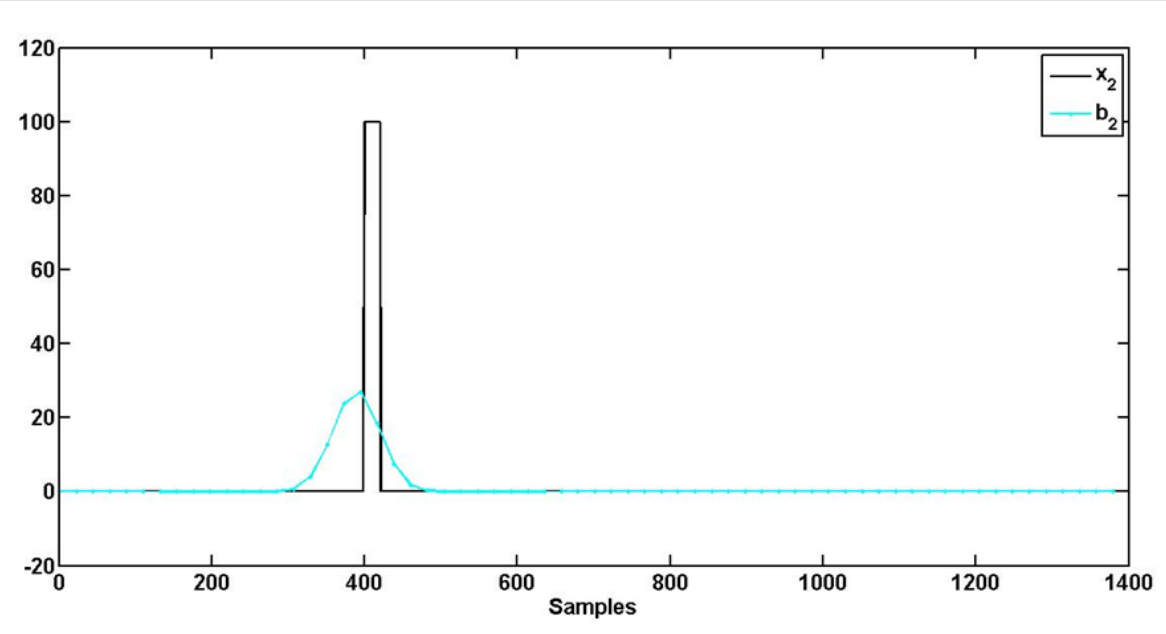

Fig. 6. Reference signal $\mathbf{x}_2$ and simulated measurements.

TABLE III

MEAN (STANDARD DEVIATION) OF THE PARAMETERS RELATED TO THE THIRD EXPERIMENT.

	c	measurements	x_{rec} in l^2	x_{rec} in $l^{1.8}$	x_{rec} in $l^{1.5}$	x_{rec} in $l^{1.2}$
h_n	$c=1$	1.004 (0.000)	0.99 (0.001)	0.99 (0.002)	0.99 (0.003)	0.99 (0.005)
	$c=2$		0.99 (0.001)	0.99 (0.002)	0.99 (0.003)	0.99 (0.005)
γ_1	$c=1$	49.2^o (0.6^o)	19.6^o (1.8^o)	17.9^o (2.3^o)	16.0^o (2.2^o)	12.4^o (2.9^o)
	$c=2$		19.6^o (1.9^o)	18.3^o (2.0^o)	16.0^o (2.1^o)	13.0^o (2.5^o)
γ_2	$c=1$	30.0^o (0.5^o)	17.1^o (1.3^o)	16.8^o (2.0^o)	15.0^o (2.1^o)	11.8^o (2.7^o)
	$c=2$		17.6^o (1.8^o)	16.8^o (2.0^o)	15.0^o (2.1^o)	11.8^o (2.7^o)
$d1$	$c=1$	1% (0.6%)	8% (2%)	8% (2%)	12% (2%)	18% (1%)
	$c=2$		7% (2%)	8% (2%)	11% (2%)	17% (1%)
$d2$	$c=1$	1% (0.6%)	8% (1%)	6% (2%)	3% (2%)	1% (1%)
	$c=2$		8% (1%)	6% (2%)	3% (2%)	1% (1%)
co	$c=1$	0.97 (0.001)	0.98 (0.002)	0.98 (0.002)	0.98 (0.002)	0.98 (0.003)
	$c=2$		0.98 (0.001)	0.98 (0.001)	0.98 (0.001)	0.98 (0.003)
W	$c=1$	67	51 (4.1)	50 (4.1)	45 (4.2)	37 (6.9)
	$c=2$		52 (4.2)	51 (4.2)	45 (4.4)	39 (6.6)

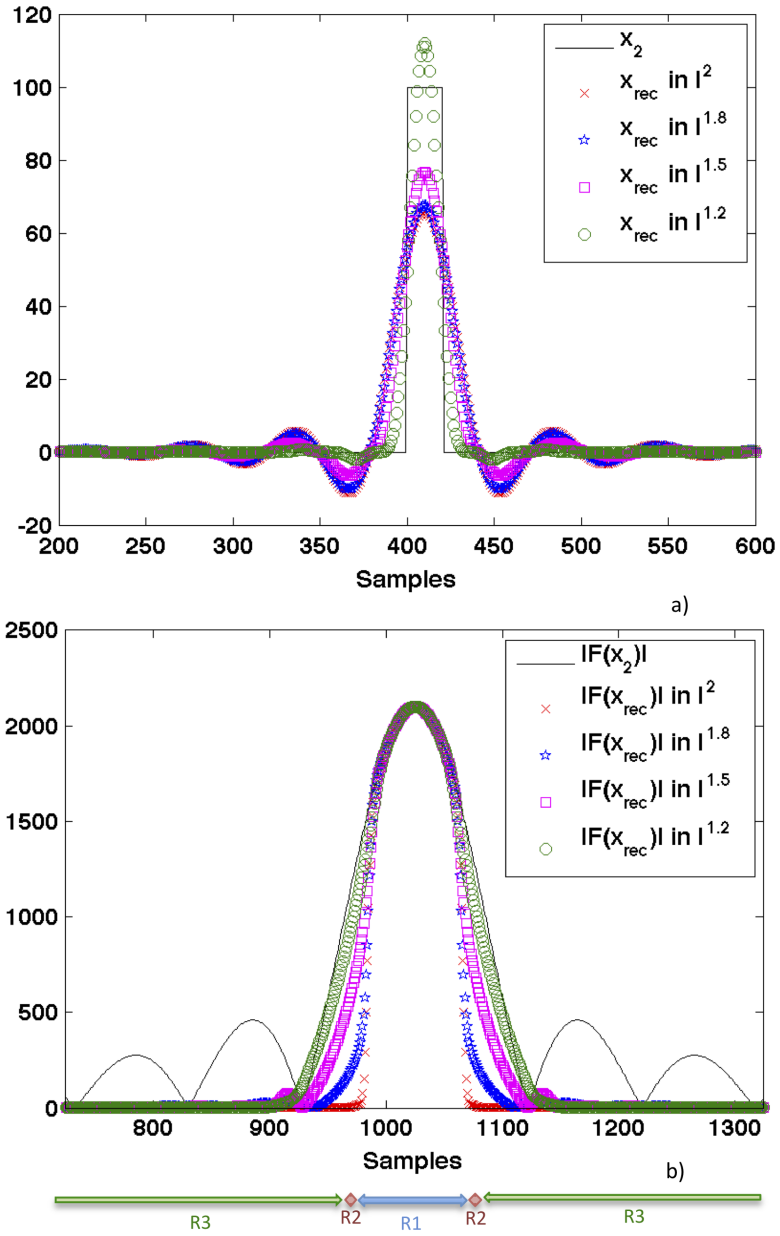

Fig. 7. (a) Reference signal (black line) and reconstructed signal in l^2 subspace (red x-mark) and in l^p subspaces with $p = 1.8$ (blue star), $p = 1.5$ (magenta square) and $p = 1.2$ (green circle), shown in the range $[200, 600]$. (b) Reference signal (black line) and reconstructed signal in l^2 subspace (red x-mark) and in l^p subspaces with $p = 1.8$ (blue star), $p = 1.5$ (magenta square) and $p = 1.2$ (green circle) in the Fourier domain. Note that R1, R2 and R3 refer to the range $[994 : 1054]$, $[972 : 993] \cup [1055 : 1076]$ and $[1 : 971] \cup [1077 : 2048]$, respectively.

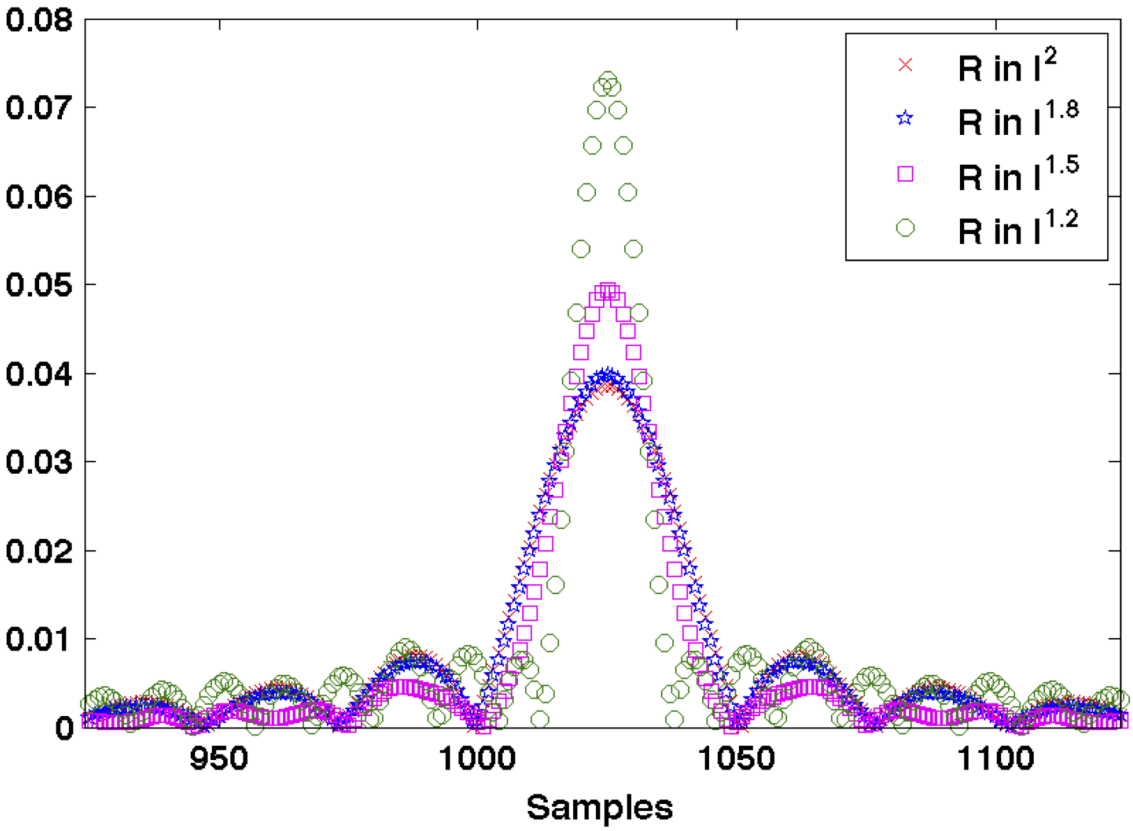

Fig. 8. The R function for $p = 2$ (red x-mark), $p = 1.8$ (blue star), 1.5 (magenta square) and 1.2 (green circle).

TABLE IV

MEAN (STANDARD DEVIATION) OF THE PARAMETERS RELATED TO THE FOURTH EXPERIMENT.

	c	measurements	x_{rec} in l^2	x_{rec} in $l^{1.8}$	x_{rec} in $l^{1.5}$	x_{rec} in $l^{1.2}$
h_n	$c=1$	0.26 (0.01)	0.44 (0.04)	0.44 (0.04)	0.53 (0.06)	0.74 (0.11)
	$c=2$		0.37 (0.02)	0.37 (0.02)	0.43 (0.03)	0.60 (0.05)
γ_1	$c=1$	80.0^o (4.8^o)	73.6^o (4.6^o)	68^o (5.9^o)	54.7^o (8.7^o)	27.5 (9.7^o)
	$c=2$		78^o (2.5^o)	75^o (3.25^o)	65.1^o (5^o)	39.1 (7.6^o)
γ_2	$c=1$	44.2^o (2.05^o)	31.5^o (3.5^o)	27.8^o (3.5^o)	21.0^o (3.5^o)	12.3^o (4.0^o)
	$c=2$		36.5^o (2.5^o)	32.9^o (2.6^o)	26.07^o (2.6^o)	16.07^o (2.4^o)
$d1$	$c=1$	–	–	–	–	–
	$c=2$		–	–	–	–
$d2$	$c=1$	1% (0.5%)	6% (2%)	4% (2%)	3% (3%)	1% (3%)
	$c=2$		4% (1%)	3% (1%)	1% (0.8%)	0.6% (0.5%)
co	$c=1$	0.53 (0.01)	0.65 (0.01)	0.69 (0.02)	0.76 (0.03)	0.87 (0.03)
	$c=2$		0.63 (0.01)	0.66 (0.01)	0.73 (0.02)	0.84 (0.02)
W	$c=1$	67	51.6 (6.3)	51.4 (6.3)	46.4 (6.2)	27 (9.3)
	$c=2$		63 (4.3)	62 (5)	56 (5.2)	39 (5.0)